

Evaluation of the Green's Function for the Mixed Potential Integral Equation (MPIE) Method in the Time Domain for Layered Media

Leung Tsang, *Fellow, IEEE*, Chong-Jin Ong, *Student Member, IEEE*, Chung-Chi Huang, and Vikram Jandhyala, *Member, IEEE*

Abstract—In the use of the time-domain integral equation (TDIE) method for the analysis of layered media, it is important to have the time-domain layered medium Green's function computed for many source-to-field distances ρ and time instants t . In this paper, a numerical method is used that computes the mixed potential Green's functions $G_v(\rho, t)$ and $G_A(\rho, t)$ for a multilayered medium for many ρ 's and t 's simultaneously. The method is applicable to multilayered media and for lossless or lossy dispersive media. Salient features of the method are: 1) the use of complex ω so that the surface wave poles are lifted off the real k_ρ axis such that pole extractions are not required; 2) the use of half-space extraction so that the integrand for the Sommerfeld integral decays exponentially along the k_ρ axis to obtain fast convergence of the integral; and 3) the use of the fast Hankel transform so that the Green's function is calculated for many values of ρ simultaneously. For a four-layer medium, we illustrate the numerical results by a three-dimensional plot of $\rho G_v(\rho, t)$ versus ρ and t and demonstrate the space-time evolution of these Green's functions. For a maximum frequency range of 8 GHz, the method requires only a few CPU minutes to compute a table of 100 (points in ρ) \times 168 (points in t) uniformly spaced values of $G_v(\rho, t)$ on an 867-MHz Pentium PC.

Index Terms—Discrete transforms, Green function, nonhomogeneous media, time-domain analysis.

I. INTRODUCTION

THE LAYERED medium Green's function in the frequency domain has been studied extensively. This was due to important applications such as geophysical probing [1] and microstrip antenna analysis [2], [3]. Early work focused on analytical techniques such as contour integration, asymptotic methods, and vertical branch cuts to evaluate the Sommerfeld integrals [4]. The focus recently is more on numerical techniques for calculating the layered medium Green's function [5]–[7]. Li *et al.* have developed a fast algorithm using the sparse-matrix/canonical grid method to solve for the impedance matrix [8]. This method uses the fast Hankel transform (FHT) [9]–[12] to speed up the evaluation of the Sommerfeld integrals and the matrix pencil (MP) method to approximate the spatial

Green's function. The drawback of the method is that pole extraction is required prior to application of the FHT, which makes the method difficult to apply to multilayered media. One method of speeding up the numerical computation of Sommerfeld integrals for layered media, where the source and field are on the surface, is the use of half-space extraction [13], [14]. This causes the integrand of the Sommerfeld integral to decay exponentially to speed up convergence significantly.

Recently, there is increasing interest in calculating the results in the time domain as many applications use wide band pulses as sources. For example, in the problem of interconnects on printed circuit boards [15], high-speed digital pulses, which span a wide frequency range, have to be analyzed on layered media to model the effects of ringing, signal delay, and crosstalk. Other important applications of time-domain analysis of layered media are the analysis of wideband microstrip antennas and the effects of ground penetration radar.

One way of solving these time-domain problems is the time-domain integral equation (TDIE) method [16], [17], as opposed to a direct discretization method like the FDTD. The TDIE is usually used with the free-space Green's function and also with images for the case of layered media. Recently, the Cagniard-de Hoop's method is used for calculating the time-domain Green's function for layered medium. However, such a method is restricted to nondispersive media and also becomes less useful for multilayered media.

It is desirable to have fast computation of the layered medium Green's function for many source-to-field distances ρ and time instants t as the TDIE requires the Green's function for many ρ 's and t 's.

In this paper, we present a method for calculation of the time domain $G_v(\rho, t)$ and $G_A(\rho, t)$ in the mixed-potential integral equation (MPIE) method for a multilayered medium where the source and field points are both on the top surface as shown in Fig. 1. The method is applicable for both lossless and lossy multilayered and dispersive media. It also calculates for many source-to-field distances ρ and many time instants t simultaneously. The salient feature of the method presented are as follows.

- 1) Complex ω is used [19], [20] so that the surface wave poles are lifted off the real k_ρ axis even for lossless medium. This removes the need for surface wave pole extraction, which can be complicated for a multilayered medium.
- 2) Half-space extraction is used so that the integrand for the non-half-space portion of the Sommerfeld integral decays

Manuscript received April 18, 2002; revised July 23, 2002. This work was supported by Intel Corporation, by the Washington Technology Center, and by the City University of Hong Kong under Research Grant 9380034.

L. Tsang is with the Department of Electronic Engineering, City University of Hong Kong, Kowloon, Hong Kong, on leave from the University of Washington, Seattle, WA 98195-2500 USA.

C.-J. Ong, C.-C. Huang, and V. Jandhyala are with the Department of Electrical Engineering, University of Washington, Seattle, WA 98195-2500 USA.

Digital Object Identifier 10.1109/TAP.2003.813631

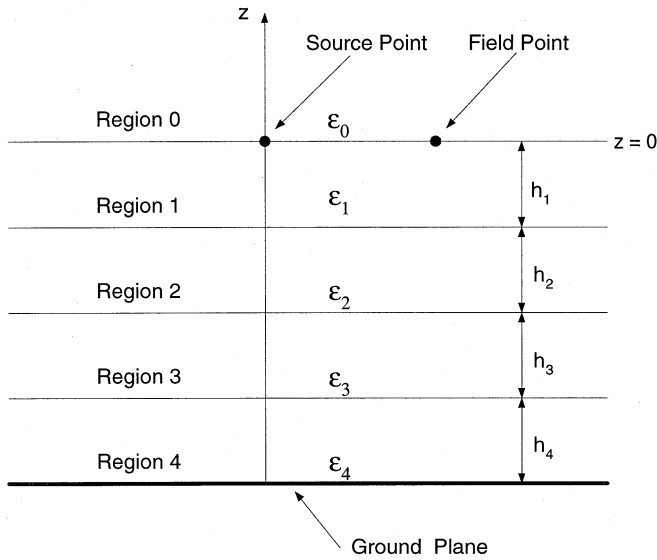


Fig. 1. A layered media. The delta source is at the origin.

exponentially along the k_ρ axis to have fast convergence of the integral. Other methods that use quasidynamic extraction have integrands that decay only as $k_\rho^{-3/2}$. Quasidynamic extraction is the extraction of the quasidynamic images. These “image” terms exist due to an approximation made for low frequencies [6].

- 3) The FHT [9] is used so that the Green’s function is calculated for many values of ρ simultaneously. This is important because the use of the time-domain Green’s function in the time-domain integral equation requires the results of many values of ρ .
- 4) The fast Fourier transform (FFT) is used for Fourier integration in ω to compute the Green’s function for many time instants t .

Although the listed methods are not new, the unique contribution of this paper is the combination of all these methods to calculate the time-domain layered media Green’s function quickly for the case where the source and the field are on the top layer.

In Section II, the evaluation of the Green’s functions in complex frequency will be presented. The Green’s function is separated into the half-space portion and the non-half-space portion. The half-space portion is evaluated by vertical branch-cut integration. The non-half-space portion is evaluated using the FHT. In Section III, the Green’s function is converted from the frequency domain to the time domain via the FFT. In Section IV, the choice of physical and numerical parameters will be discussed. We discuss the choice of $\text{Im}(\omega)$ and the sampling intervals and domain of k_ρ and ω such that one set of numerical parameters give results that are accurate for all values of ρ and t in the specified range. The choice of $\text{Im}(s)$ for the FHT will also be described. In Section V, the numerical result for $G_v(\rho, \omega)$ is shown as a function of ρ for a single-layer medium and as a function of frequency for a four-layer medium. We also show $G_A(\rho, t)$ and $G_v(\rho, t)$ for the four-layer medium as functions of time t for the case where complex frequency is used and the case where real frequency is employed to show that the two methods are in good agreement. To illustrate the technique for calculating

$G_v(\rho, t)$ for many values of ρ and t simultaneously, we generate a three-dimensional (3-D) mesh of $\rho G_v(\rho, t)$ versus ρ and t . It is shown that it requires only a few CPU minutes using Matlab to compute a table of 100 (points in ρ) \times 168 (points in t) uniformly spaced values of $G_v(\rho, t)$.

II. EVALUATION OF $G_A(\rho, \omega)$ AND $G_v(\rho, \omega)$ IN THE COMPLEX FREQUENCY DOMAIN

Let the surface current \vec{J}_s be confined to a surface sheet in the xy -plane and let the surface charge be ρ_s . The Green’s functions for the vector magnetic potential \vec{A} and the scalar electric potential Φ can be defined as follows:

$$\begin{aligned}\vec{A}(\vec{r}) &= \iint G_A(\vec{r}, \vec{r}') \vec{J}_s(\vec{r}') dx' dy' \\ \Phi(\vec{r}) &= \iint G_v(\vec{r}, \vec{r}') \rho_s(\vec{r}') dx' dy'.\end{aligned}$$

For a multilayered medium shown in Fig. 1, G_A and G_v are given by

$$\begin{aligned}G_A(\rho, \omega) &= -j \frac{\mu_0}{4\pi} \int_0^\infty dk_\rho \frac{k_\rho}{k_z} J_0(k_\rho \rho) (1 + R^{\text{TE}}) \quad (1) \\ G_v(\rho, \omega) &= -\frac{j}{4\pi\epsilon_0} \int_0^\infty dk_\rho \frac{1}{k_z} \\ &\quad \times \left[k_\rho + \frac{k_0^2 R^{\text{TE}} + k_z^2 R^{\text{TM}}}{k_\rho} \right] J_0(k_\rho \rho) \quad (2)\end{aligned}$$

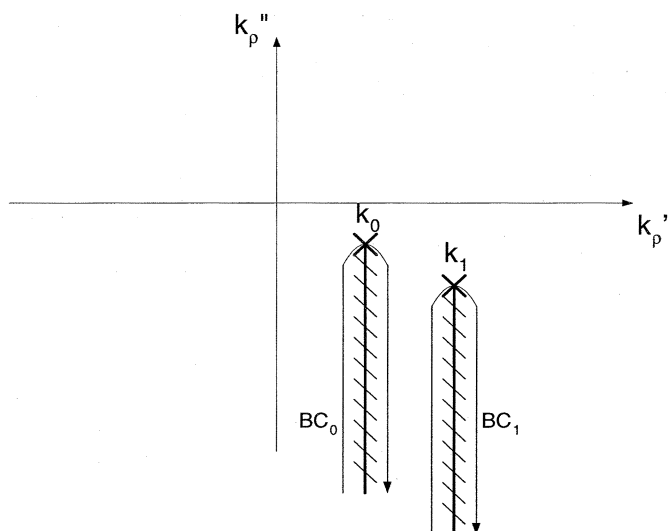
where $\rho = \sqrt{x^2 + y^2}$, $k_\rho = \sqrt{k_x^2 + k_y^2}$, and $k_z = \sqrt{k_0^2 - k_\rho^2}$. R^{TE} and R^{TM} are the transverse electric (TE) and transverse magnetic (TM) reflection coefficients, respectively, due to a plane wave incident on the multilayered medium. R^{TE} and R^{TM} can be calculated from equations found in [20].

It is apparent that (1) and (2) cannot be integrated directly as there are surface wave poles on the k_ρ axis. One way of overcoming this difficulty is to add a small imaginary component to the angular frequency ω to extend $G_A(\rho, \omega)$ and $G_v(\rho, \omega)$ to the complex frequency. Let $\omega = \omega' + j\omega''$ with $\omega'' < 0$ [19], [20]. In this manner, the poles will be shifted off the real k_ρ axis. Subsequently, the inverse Fourier transform is taken in the complex ω plane. Thus, the imaginary component of ω is compensated in the time domain by multiplying the Fourier transformed results of G_A and G_v by an exponential factor.

A. Half-Space Extraction of $G_A(\rho, \omega)$ and $G_v(\rho, \omega)$

An efficient way to evaluate (1) and (2) is to extract the half space. This means that the components of R^{TE} and R^{TM} due to layers 0 and 1 only are evaluated separately, assuming that layer 1 is infinitely deep. Because the angular frequency ω is complex, the integration for the non-half-space portion can then be performed on the real k_ρ axis

$$G_A(\rho, \omega) = G_A^{(H)}(\rho, \omega) + G_A^{(N)}(\rho, \omega)$$


 Fig. 2. Branch-cut integration paths for evaluation of $G_v^{(H)}(\rho, \omega)$.

where

$$G_A^{(H)}(\rho, \omega) = -\frac{j\mu_0}{4\pi} \int_0^\infty dk_\rho \frac{k_\rho}{k_z} J_0(k_\rho \rho) (1 + R_{01}^{\text{TE}})$$

$$G_A^{(N)}(\rho, \omega) = -\frac{j\mu_0}{4\pi} \int_0^\infty dk_\rho \frac{k_\rho}{k_z} J_0(k_\rho \rho) (R^{\text{TE}} - R_{01}^{\text{TE}}) \quad (3)$$

$$G_v(\rho, \omega) = G_v^{(H)}(\rho, \omega) + G_v^{(N)}(\rho, \omega)$$

where

$$G_v^{(H)}(\rho, \omega) = -\frac{j}{4\pi\epsilon_0} \int_0^\infty dk_\rho \frac{1}{k_z}$$

$$\times \left[k_\rho + \frac{k_0^2 R_{01}^{\text{TE}} + k_z^2 R_{01}^{\text{TM}}}{k_\rho} \right] J_0(k_\rho \rho)$$

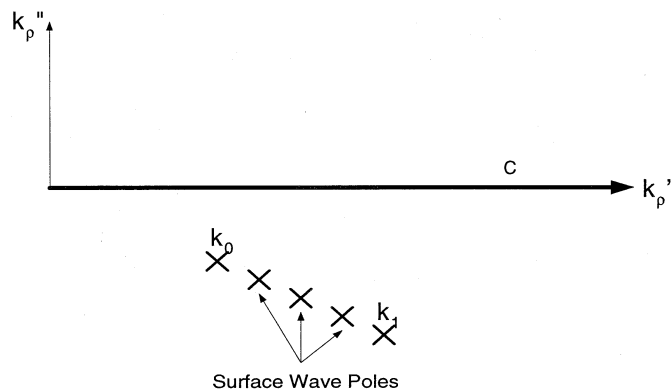
$$G_v^{(N)}(\rho, \omega) = -\frac{j}{4\pi\epsilon_0} \int_0^\infty dk_\rho \frac{1}{k_z} J_0(k_\rho \rho)$$

$$\times \left[\frac{k_0^2 (R^{\text{TE}} - R_{01}^{\text{TE}}) + k_z^2 (R^{\text{TM}} - R_{01}^{\text{TM}})}{k_\rho} \right]. \quad (4)$$

R_{01}^{TE} and R_{01}^{TM} are the reflection coefficients for TE- and TM-polarized waves, respectively, incident on the boundary between layers 0 and 1, where layer 1 is infinitely thick.

The half-space portion is extracted instead of the free space portion, despite having a closed form for the latter. This is because the integrand for the non-half-space portion decays exponentially with k_ρ , whereas the integrand for the non-free space portion decays as a power of k_ρ . This affects the size of the domain of k_ρ required for the FHT.

The integrals for $G_A^{(H)}$ and $G_v^{(H)}$ can be evaluated by integrating along the vertical branch cuts with branch points at $k_\rho = k_0 = (\omega' + j\omega'')\sqrt{\mu\epsilon_0}$ and $k_\rho = k_1 = (\omega' + j\omega'')\sqrt{\mu\epsilon_1}$ [14]. The branch-cut integration paths are shown in Fig. 2. The integrals for $G_A^{(H)}(\rho, \omega)$ and $G_v^{(H)}(\rho, \omega)$ converge very quickly. Details for the branch-cut integration for $G_v^{(H)}$ are found in


 Fig. 3. Integration path for $G_v^{(N)}(\rho, \omega)$.

Appendix I-A. The integrals for $G_A^{(N)}(\rho, \omega = \omega' + j\omega'')$ and $G_v^{(N)}(\rho, \omega = \omega' + j\omega'')$ can be evaluated along the real k_ρ axis.

B. FHT for Evaluation of $G_A^{(N)}(\rho, \omega)$ and $G_v^{(N)}(\rho, \omega)$

Using complex frequency, the poles are moved off the real k_ρ axis as shown in Fig. 3. The integrands for $G_A^{(N)}(\rho, \omega)$ and $G_v^{(N)}(\rho, \omega)$ are analytic functions that can be evaluated using the FHT [9].

Let the general form of (3) and (4) be

$$f(\rho) = \int_0^\infty F(k_\rho) k_\rho J_\nu(k_\rho \rho) dk_\rho. \quad (5)$$

Let ρ and k_ρ be logarithmically spaced vectors such that

$$\rho = R \exp(ax) \quad (6)$$

$$k_\rho = K \exp(-ay) \quad (7)$$

where x and y are linearly spaced vectors.

Let

$$H_\nu(x - y) = e^{a(x-y)} J_\nu \left(K R e^{a(x-y)} \right)$$

$$G(y) = K e^{-ay} F(K e^{-ay}).$$

Equation (5) becomes a convolution integral of the form

$$f(\rho) = K a e^{-ax} \int_{-\infty}^\infty dy H_\nu(x - y) G(y).$$

This convolution can be efficiently solved using the Fourier transform. Let

$$\tilde{H}_\nu(s) = \int_{-\infty}^\infty dy e^{-j2\pi y s} H_\nu(y) \quad (8)$$

$$\tilde{G}(s) = \int_{-\infty}^\infty dy e^{-j2\pi y s} G(y). \quad (9)$$

A closed form exists for (8)

$$\tilde{H}_\nu(s) = \frac{1}{aKR} \left(\frac{2}{KR} \right)^{-j\frac{2\pi s}{a}} \frac{\Gamma\left(\frac{\nu+1}{2} - \frac{j\pi s}{a}\right)}{\Gamma\left(\frac{\nu+1}{2} + \frac{j\pi s}{a}\right)}.$$

$\tilde{G}(s)$ can be evaluated using the FFT. It is important that $G(y)$ is effectively captured in the FFT window. In Section IV-B-2, the choice of $\text{Im}(s)$ for the FHT is described.

III. TRANSFORMING $G_A(\rho, \omega)$ AND $G_v(\rho, \omega)$ TO THE TIME DOMAIN

$G_A(\rho, \omega)$ and $G_v(\rho, \omega)$ are usually not frequency limited within the frequency band of interest. It is necessary to introduce a frequency-limited source function to limit the frequency range of the Fourier integration. Let the source function be a Gaussian pulse function given by

$$x(t) = \frac{1}{\sqrt{\pi}\tau} \exp\left[-\left(\frac{t-t_0}{\tau}\right)^2\right].$$

The Fourier transform of $x(t)$ is

$$X(\omega) = \exp(-j\omega t_0) \exp\left(-\frac{\omega^2 \tau^2}{4}\right)$$

where t_0 is at the peak of the pulse function and τ is a measure of the pulsewidth.

Thus $G_{A,v}(\rho, t)$ can be evaluated from the Fourier transform of the product of $X(\omega)$ and $G_{A,v}(\rho, \omega)$. If $\omega = \omega' + j\omega''$, then

$$G_{A,v}(\rho, t) = \frac{e^{-\omega'' t}}{2\pi} \int_{-\infty}^{\infty} d\omega' e^{j\omega' t} X(\omega' + j\omega'') \times G_{A,v}(\rho, \omega' + j\omega'').$$

Since

$$X(-\omega' + j\omega'') G_{A,v}(\rho, -\omega' + j\omega'') = [X(\omega' + j\omega'') G_{A,v}(\rho, \omega' + j\omega'')]^*.$$

It follows that

$$G_{A,v}(\rho, t) = \frac{e^{-\omega'' t}}{\pi} \times \text{Re} \left[\int_0^{\infty} d\omega' e^{j\omega' t} X(\omega' + j\omega'') G_{A,v}(\rho, \omega' + j\omega'') \right]. \quad (10)$$

This result is logical, as we expect the function $G_{A,v}$ to be real in the time domain. The Fourier integral for $G_{A,v}(\rho, t)$ can be efficiently evaluated using the FFT. In the FFT, the largest value of ω needed, denoted by ω_{\max} , is determined by $X(\omega)$.

The results of $G_{A,v}(\rho, \omega)$ for real ω can be generated by taking the FFT of $G_v(\rho, t)$ and dividing by $X(\omega)$.

IV. NUMERICAL IMPLEMENTATION

In this section, details will be provided on the choice of numerical parameters for calculation of the numerical solution. A single choice of numerical parameters is necessary for the entire range of ρ and t specified.

A. Physical Parameters

The three physical parameters of the problem (aside from the material dimensions and properties) are

- 1) ω_{\max} , the maximum angular frequency;
- 2) ρ_{\max} , the maximum distance from the source to the field point (on the same plane);
- 3) t_{\max} , the maximum time instant desired.

The maximum time evaluated will depend on the number of frequency points N_ω and the angular frequency spacing $\Delta\omega'$

$$t_{\max} = \frac{2\pi(N_\omega - 1)}{N_\omega \Delta\omega'}.$$

B. Numerical Parameters

1) *Choice of $\text{Im}(\omega)$* : From (10), it is seen that a term $e^{-\omega'' t}$ must be multiplied with the Fourier integral to get the value of $G_{A,v}(\rho, t)$. Since ω'' is negative, $|\omega'' t_{\max}|$ must be small so that numerical errors will not occur in the final result. Furthermore, ω'' affects the distance the surface wave poles are lifted from the k_ρ axis. If ω'' is too small, the FHT will be evaluated too close to the poles, resulting in inaccurate results.

Let

$$\omega'' t_{\max} = -0.3$$

$$\omega'' = -\frac{0.3}{t_{\max}}.$$

2) *Choice of $\text{Im}(s)$ for the FHT*: Referring to (8) and (9), it is useful to have an imaginary part of s to ensure convergence of the Fourier integrals. Let $s = s' + js''$.

To ensure convergence of $\tilde{H}_\nu(s)$

$$-\frac{a}{2\pi} < s'' < -\frac{a}{4\pi}. \quad (11)$$

To ensure convergence of $\bar{G}(s)$

$$s'' < \frac{a}{2\pi}. \quad (12)$$

Refer to Appendix II for the derivation of the two inequalities. Since (11) is more restrictive than (12), (11) is the range for s'' . The second author has found that $s'' = -a/4\pi$ works quite well in practice.

3) *Choice of Other Numerical Parameters for k_ρ and ρ for the FHT*: The following are guidelines for the choice of the domain for k_ρ :

$$a = 0.0003$$

$$k_{\rho \max} = \max\left(5k_{\max}, \frac{10}{h}\right)$$

$$y_{\min} = -\frac{1}{a} \log\left(\frac{1}{a}\right)$$

$$y_{\max} = -2y_{\min}$$

$$\mathbf{x} = \mathbf{y}.$$

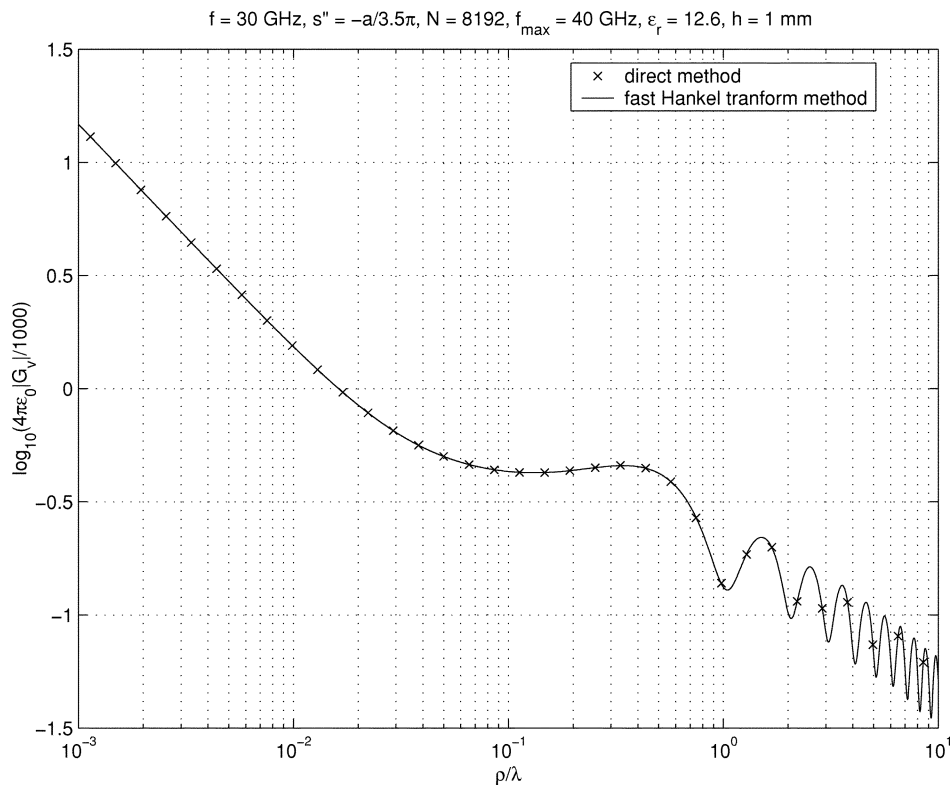


Fig. 4. Comparison between the amplitude of scalar potential $G_v(\rho, \omega)$ with $G_v^{(N)}$ computed from direct numerical integration and the FHT. Relative permittivity of substrate $\epsilon_r = 12.6$, substrate thickness $h = 1$ mm, and frequency $f = 30$ GHz.

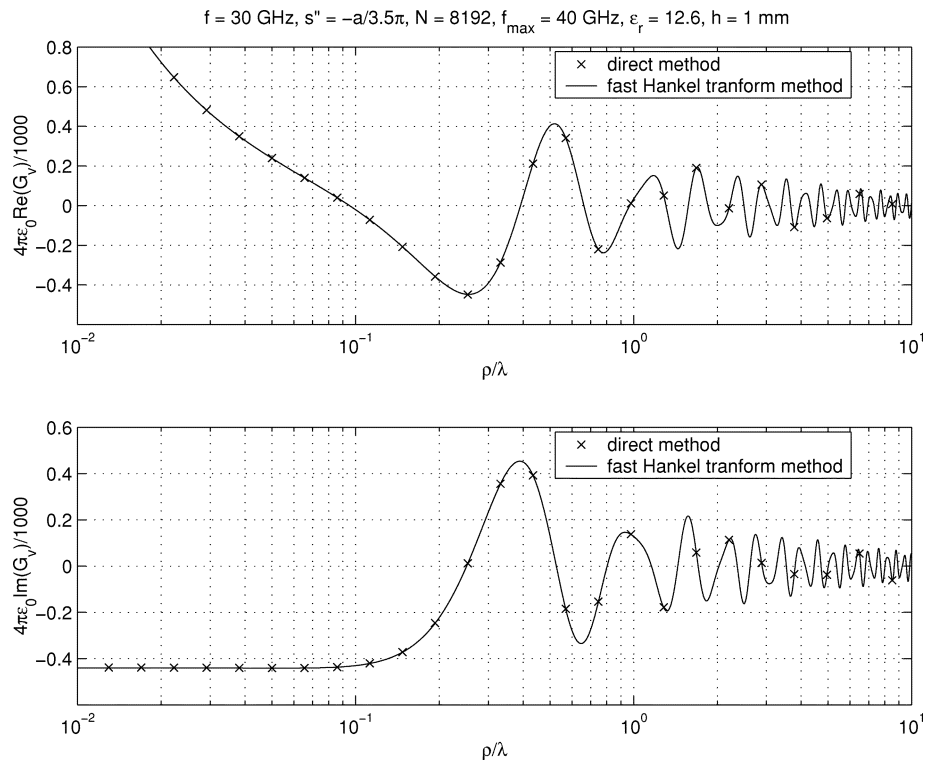


Fig. 5. Comparison between the real and imaginary part of the scalar potential $G_v(\rho, \omega)$ with $G_v^{(N)}$ computed from direct numerical integration and the FHT. Relative permittivity of substrate $\epsilon_r = 12.6$, substrate thickness $h = 1$ mm, and frequency $f = 30$ GHz.

h is the thickness of each layer. $k_{\rho \max}$ was chosen with the consideration that after half-space extraction, the integrand for the non-half-space portion of the Green's functions decay exponentially as $\exp(-2k_{\rho}h)$. Note that \mathbf{x} and \mathbf{y} are linearly spaced vec-

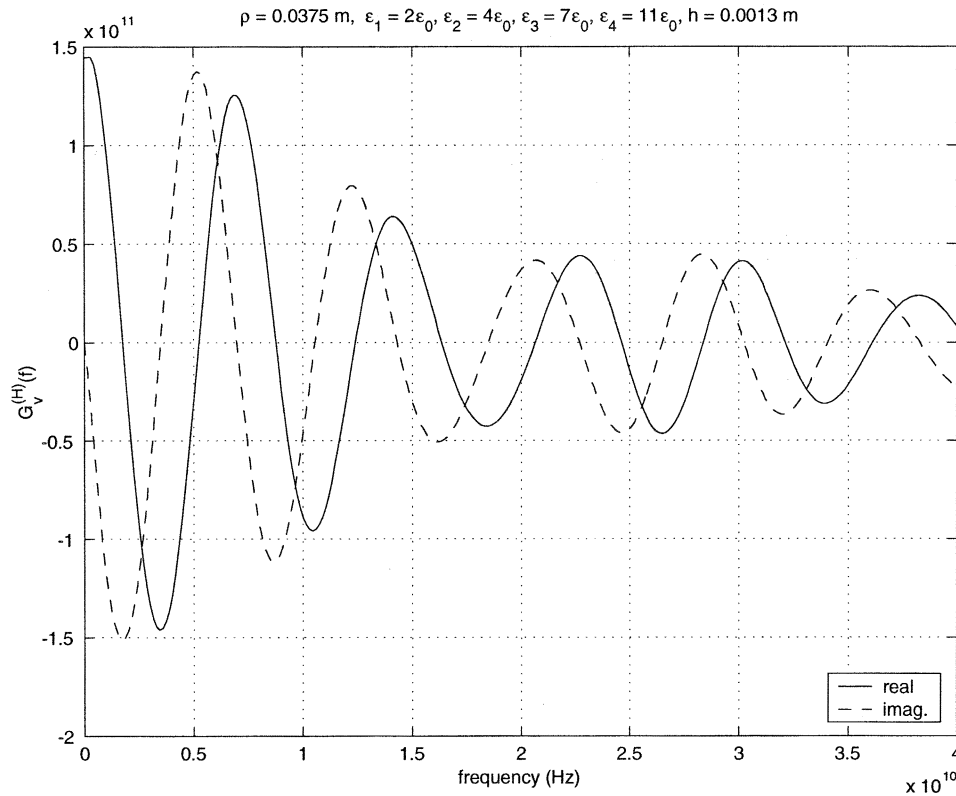


Fig. 6. Real and imaginary parts of $G_v^{(H)}(\rho, \omega)$ as a function of frequency. Source-to-field distance $\rho = 3.75$ cm, permittivity of dielectric layers $\epsilon_1 = 2\epsilon_0$, $\epsilon_2 = 4\epsilon_0$, $\epsilon_3 = 7\epsilon_0$, $\epsilon_4 = 11\epsilon_0$, and thickness of each dielectric layer $h = 1.3$ mm.

tors. The second author chose the number of points for the FHT to be 8192.

The range of ρ is determined from ρ_{\max} , the maximum source-to-field distance required. From (6), it can be deduced that

$$R = \rho_{\max} \exp(-ax_{\max}).$$

4) *Choice of Numerical Parameters for Frequency and Time:* The method for estimating $\Delta\omega'$ is based on the maximum time of the signal t_{limit} that needs to be evaluated. (After t_{limit} , the signal can be considered to have zero value.) To prevent aliasing in the time-domain

$$\Delta\omega' \leq \frac{2\pi}{2t_{\text{limit}}} = \frac{\pi}{t_{\text{limit}}}.$$

The number of points in ω is given by

$$N_{\omega} = \text{round} \left(\frac{2\omega_{\max}}{\Delta\omega'} \right).$$

The time spacing and the maximum time interval are determined from $\Delta\omega'$ and N_{ω}

$$\Delta t = \frac{2\pi}{N_{\omega} \Delta\omega'}$$

$$t_{\max} = (N_{\omega} - 1) \Delta t.$$

V. NUMERICAL RESULTS

A. FHT for $G_v(\rho, \omega)$ as a Function of ρ Using Complex Frequency

The results shown will be mainly for G_v . The results for G_A can be obtained in a similar manner. The FHT is tested using complex frequency. Figs. 4 and 5 show $G_v(\rho, \omega)$ against ρ for $G_v^{(N)}$ computed using the direct numerical integration and FHT. The comparison between the two sets of results is excellent. The parameters for testing are similar to that found in [8]. The dielectric constant is $\epsilon_r = 12.6$, the thickness of the dielectric layer is $h = 1$ mm and the operating frequency is $f = 30$ GHz. The substrate is a single dielectric layer with a perfect electric-conducting ground plane beneath. The imaginary part of the angular frequency ω is $\omega'' = -0.3(f_{\max}/50)$, where f_{\max} is chosen as 40 GHz. The FHT is performed using 8192 points in k_{ρ} with $\text{Im}(s) = -(a/3.5\pi)$.

B. Evaluation of $G_v(\rho, \omega)$ as a Function of Frequency

Fig. 6 shows the real and imaginary parts of $G_v^{(H)}(\rho, \omega)$ calculated using complex ω and half-space extraction. The physical parameters used for testing are: $\rho = 3.75$ cm, $\epsilon_1 = 2\epsilon_0$, $\epsilon_2 = 4\epsilon_0$, $\epsilon_3 = 7\epsilon_0$, $\epsilon_4 = 11\epsilon_0$, and $h = 1.3$ mm. The substrate is a four-layer dielectric with a perfect electric conducting ground plane below the fourth layer. The branch-cut lengths are set at $10/h$.

Fig. 7 shows the real and imaginary parts of $G_v^{(N)}(\rho, \omega)$ calculated using direct numerical integration and the FHT. The FHT evaluated 8192 points in ρ and cubic spline was used to

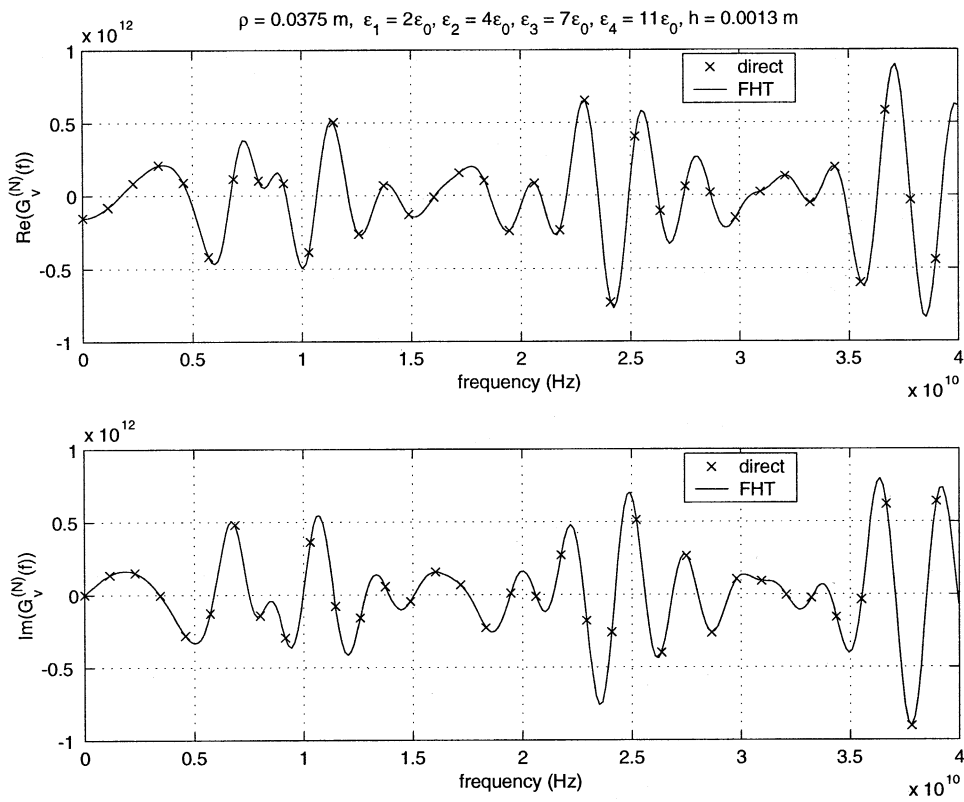


Fig. 7. Real and Imaginary parts of $G_v^{(N)}(\rho, \omega)$ as a function of frequency. Source-to-field distance $\rho = 3.75 \text{ cm}$, permittivity of dielectric layers $\epsilon_1 = 2\epsilon_0$, $\epsilon_2 = 4\epsilon_0$, $\epsilon_3 = 7\epsilon_0$, $\epsilon_4 = 11\epsilon_0$, and thickness of each dielectric layer $h = 1.3 \text{ mm}$.

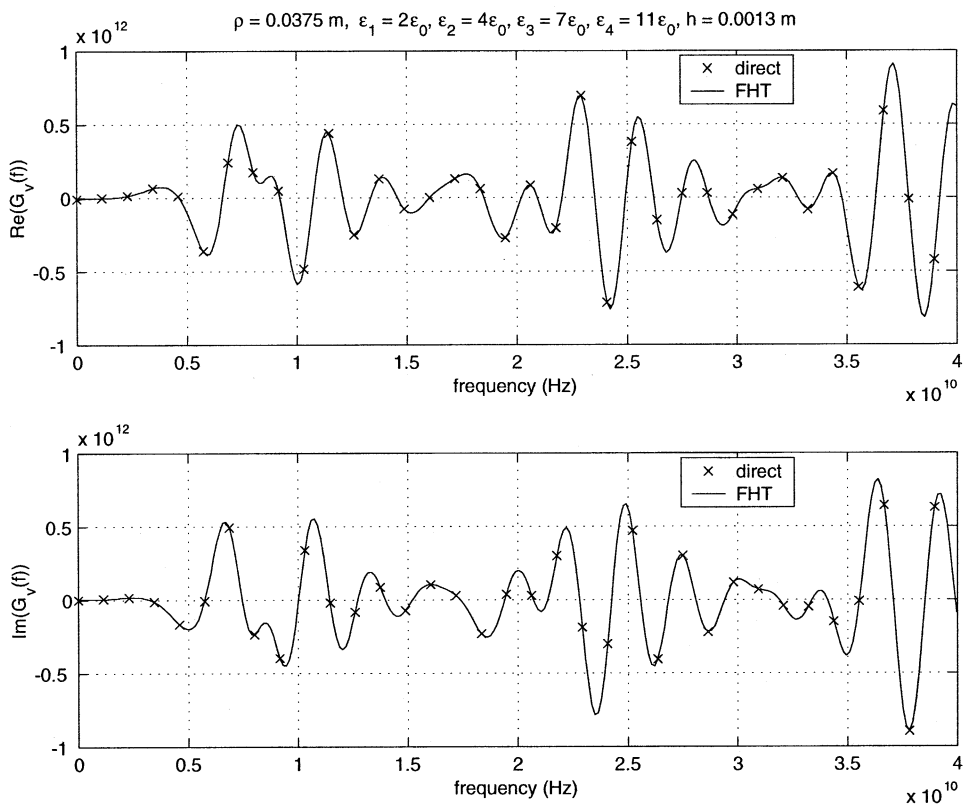


Fig. 8. Real and Imaginary parts of $G_v(\rho, \omega)$ as a function of frequency. Source-to-field distance $\rho = 3.75 \text{ cm}$, permittivity of dielectric layers $\epsilon_1 = 2\epsilon_0$, $\epsilon_2 = 4\epsilon_0$, $\epsilon_3 = 7\epsilon_0$, $\epsilon_4 = 11\epsilon_0$, and thickness of each dielectric layer $h = 1.3 \text{ mm}$.

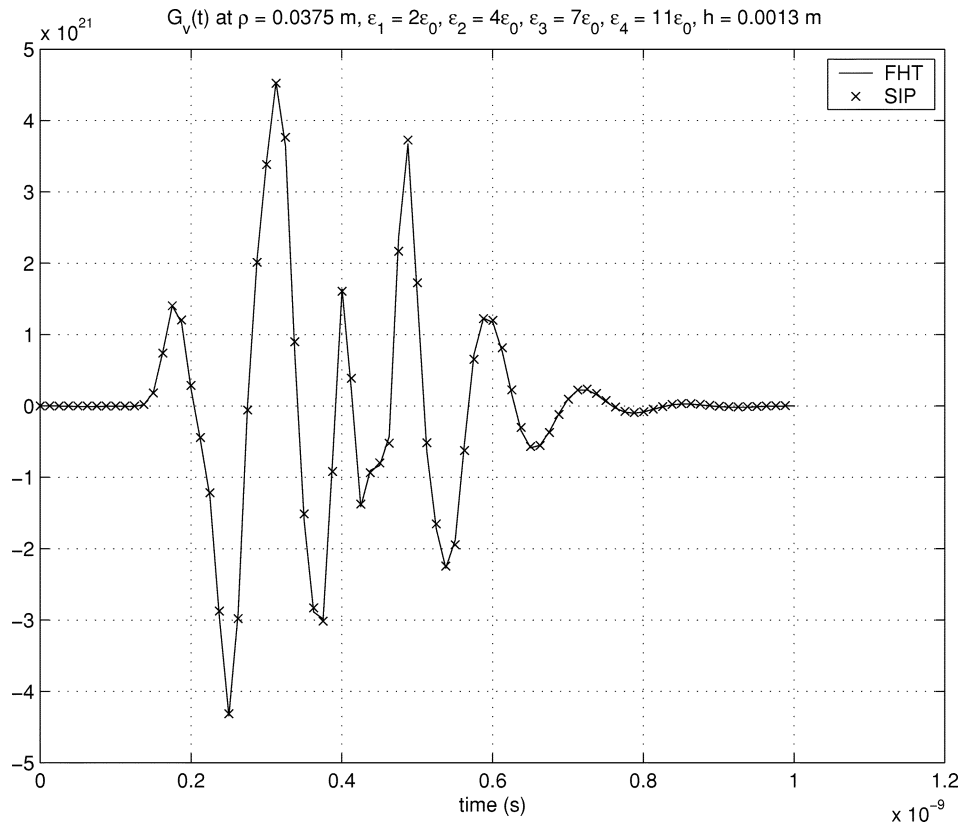


Fig. 9. $G_v(\rho, t)$ as a function of time. Source-to-field distance $\rho = 3.75$ cm, permittivity of dielectric layers $\epsilon_1 = 2\epsilon_0$, $\epsilon_2 = 4\epsilon_0$, $\epsilon_3 = 7\epsilon_0$, $\epsilon_4 = 11\epsilon_0$, thickness of each dielectric layer $h = 1.3$ mm, and pulsewidth $\tau = 20$ ps.

interpolate the value at $\rho = 3.75$ cm. The value of $\text{Im}(s) = -a/3.99\pi$. The agreement between the results calculated from the two methods is excellent. The maximum relative error is 0.859%. The mean relative error was 0.252%. The parameters used are the same as for the $G_v^{(N)}(\rho, \omega)$ case.

Fig. 8 shows the real and imaginary parts of $G_v(\rho, \omega)$, which is the sum of $G_v^{(H)}(\rho, \omega)$ and $G_v^{(N)}(\rho, \omega)$. For the graph labeled “direct”, the $G_v^{(N)}(\rho, \omega)$ portion is computed using numerical integration instead of the FHT.

C. Evaluation of $G_v(\rho, t)$ and $G_A(\rho, t)$ as a Function of Time

Fig. 9 shows $G_v(\rho, t)$ as a function of time. This is the $G_v(\rho, \omega)$ shown in the previous subsection that has been multiplied by $X(\omega)$ and fast Fourier transformed. The parameters used for $X(\omega)$ are $\tau = 20$ ps and $t_0 = 2.5\tau$. The comparison is made with a $G_v(\rho, t)$ function that is evaluated in frequency domain using real ω and with $G_v^{(N)}(\rho, \omega)$ integrated along the Sommerfeld integration path (SIP), as shown in Fig. 10. The comparison $G_v(\rho, t)$ function is Fourier transformed using direct numerical Fourier integration rather than the FFT. The agreement between the two sets of results is excellent.

Fig. 11 shows $G_A(\rho, t)$ as a function of time. $G_A(\rho, t)$ is obtained in a similar way to $G_v(\rho, t)$. The agreement between the two sets of results is excellent. Small errors can be seen in the two sets of results. The main source of error is aliasing. The time-domain Green’s function is actually not limited in time if a frequency limit is imposed. A time limit must be approximated so that a frequency sampling interval can be obtained. Sampling

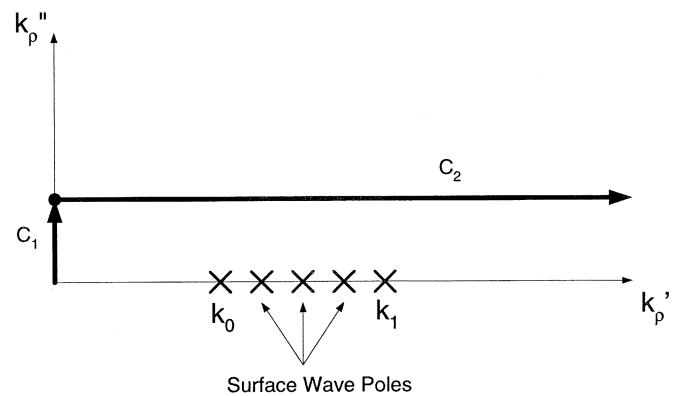


Fig. 10. The SIP.

more points in frequency is likely to increase the accuracy but lengthen the run time of the algorithm.

Fig. 12 shows $\rho G_v(\rho, t)$ as a function of both ρ and t . The pulsewidth τ used was 100 ps. The maximum frequency was set at 8 GHz. The same four-layer multilayer medium described in the previous section was used. $\rho G_v(\rho, t)$ was evaluated for 100 points in ρ and 168 points in t . The results took 2 min and 51 s to evaluate in Matlab (to within a relative error of 10^{-3} for the branch-cut integrations) on an 867-MHz Pentium PC. In comparison, using real frequency and numerical integration, generating the same mesh to the same accuracy would take approximately 3 h. The results show the space-time evolution of $G_v(\rho, t)$.

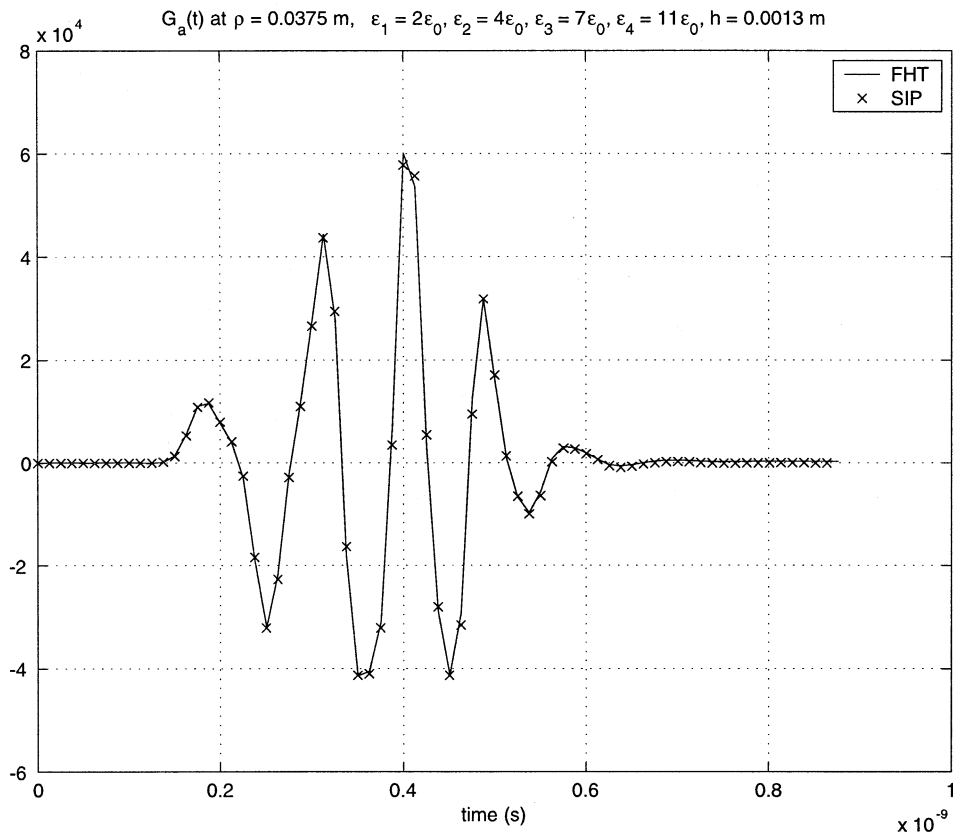


Fig. 11. $G_A(\rho, t)$ as a function of time. Source-to-field distance $\rho = 3.75$ cm, permittivity of dielectric layers $\epsilon_1 = 2\epsilon_0, \epsilon_2 = 4\epsilon_0, \epsilon_3 = 7\epsilon_0, \epsilon_4 = 11\epsilon_0$, thickness of each dielectric layer $h = 1.3$ mm, and pulsewidth $\tau = 20$ ps.

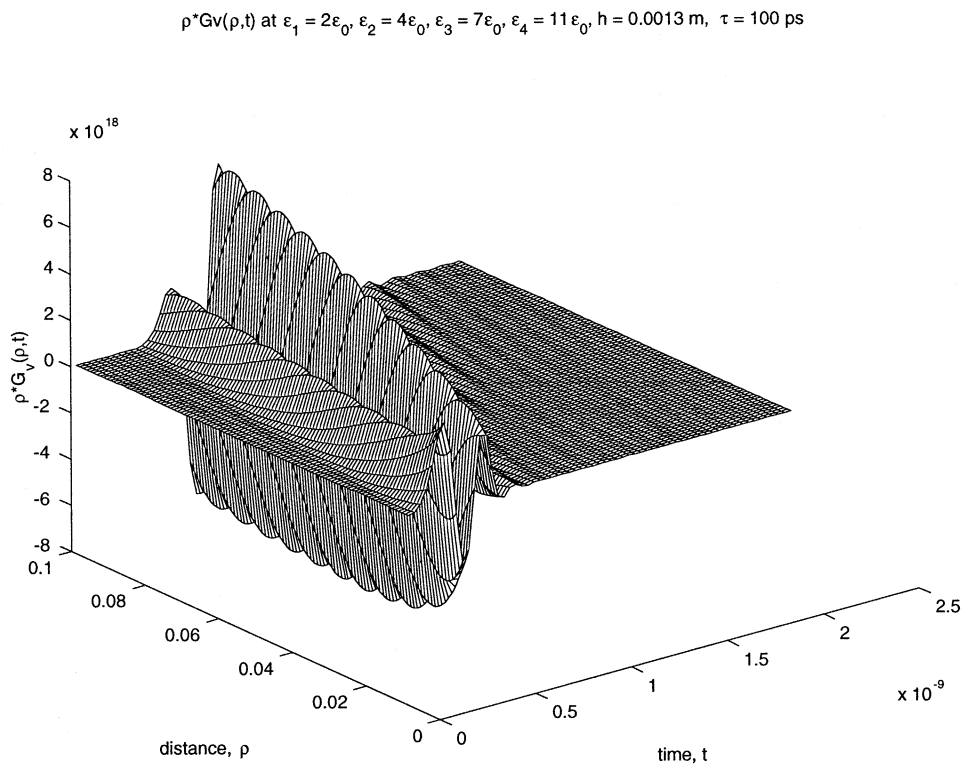


Fig. 12. 3-D mesh of $\rho G_v(\rho, t)$ as a function of both ρ and t . Permittivity of dielectric layers $\epsilon_1 = 2\epsilon_0, \epsilon_2 = 4\epsilon_0, \epsilon_3 = 7\epsilon_0, \epsilon_4 = 11\epsilon_0$, thickness of each dielectric layer $h = 1.3$ mm, and pulsewidth $\tau = 100$ ps.

VI. CONCLUSION

This paper has shown a new method for calculating $G_A(\rho, t)$ and $G_v(\rho, t)$, the time-domain layered media Green's function for the MPIE, for the case where the source and field points are on the top layer. This method uses complex ω to shift the poles off the real k_ρ axis as opposed to extracting the poles. It also uses half-space extraction to cause the integrand of the non-half-space portion to decay exponentially with k_ρ . The branch-cut integration technique is used to evaluate the half-space portion. The non-half space portion is evaluated using the FHT. The FFT is used to transform the Green's function to the time domain. This method can efficiently calculate $G_A(\rho, t)$ and $G_v(\rho, t)$ for many source-to-field distances ρ and time instants t simultaneously. The physical and numerical parameters for the method are shown. The FHT method had been validated for $G_v^{(N)}(\rho, \omega)$ by comparison with direct numerical integration. The $G_A(\rho, t)$ and $G_v(\rho, t)$ results are validated by comparison with results obtained by using real ω and direct numerical Fourier integration. A 3-D mesh of $\rho G_v(\rho, t)$ was generated with little CPU requirement. The results of $G_v(\rho, \omega)$ for real ω can be generated by taking the FFT of $G_v(\rho, t)$ and dividing by $X(\omega)$. The authors are presently applying the method described in this paper to a lossy dispersive medium with a lossy conductor.

APPENDIX I

BRANCH-CUT INTEGRATION FOR EVALUATION OF HALF-SPACE PORTIONS OF THE MPIE GREEN'S FUNCTIONS

A. Branch-Cut Integration for $G_v^{(H)}$

Let

$$G_v^{(H)}(\rho, \omega) = -\frac{j}{4\pi\epsilon_0} \int_0^\infty dk_\rho J_0(k_\rho \rho) f(k_\rho)$$

where

$$f(k_\rho) = \frac{1}{k_z} \left[k_\rho + \frac{k_0^2 R_{01}^{\text{TE}} + k_z^2 R_{01}^{\text{TM}}}{k_\rho} \right].$$

With reference to k_ρ , $k_z = \sqrt{k_0^2 - k_\rho^2}$ is an even function. Since R^{TE} and R^{TM} are functions of k_z , they are also even functions with respect to k_ρ . Thus $f(k_\rho)$ is an odd function of k_ρ . By using the reflection formula $H_0^{(1)}(e^{-j\pi}x) = -H_0^{(2)}(x)$ ¹ [20]

$$\begin{aligned} \therefore \int_0^\infty dk_\rho J_0(k_\rho \rho) f(k_\rho) &= \frac{1}{2} \int_{-\infty}^\infty dk_\rho H_0^{(2)}(k_\rho \rho) f(k_\rho) \\ \therefore G_v^{(H)}(\rho, \omega) &= -\frac{j}{8\pi\epsilon_0} \int_{-\infty}^\infty dk_\rho \\ &\times \left[\frac{k_\rho}{k_z} + \frac{k_0^2}{k_z k_\rho} \left(\frac{\mu_1 k_z - \mu_0 k_{1z}}{\mu_1 k_z + \mu_0 k_{1z}} \right) \right. \\ &\quad \left. + \frac{k_z}{k_\rho} \left(\frac{\epsilon_1 k_z - \epsilon_0 k_{1z}}{\epsilon_1 k_z + \epsilon_0 k_{1z}} \right) \right] \\ &\times H_0^{(2)}(k_\rho \rho). \end{aligned}$$

¹This formula may come as a surprise to some, since $J_0(x)$ is an even function. The explanation is that $Y_0(x)$ is complex valued for negative values of x .

TABLE I
PROPERTIES OF VERTICAL BRANCH CUTS

	k_z	k_{1z}
BC_0	$(k_z)_L = -(k_z)_R$ $\text{Re}(k_z)_R \leq 0$ and $\text{Im}(k_z)_R \leq 0$	analytic $\text{Re}(k_{1z}) > 0$ and $\text{Im}(k_{1z}) < 0$
BC_1	analytic $\text{Im}(k_{1z}) > 0$	$(k_{1z})_L = -(k_{1z})_R$ $\text{Re}(k_{1z})_R \leq 0$ and $\text{Im}(k_{1z})_R \leq 0$

The properties of the vertical branch cuts arising from the poles at k_z and k_{1z} are summarized in Table I.

1) *Integration on Branch-Cut 0:* Note that $k_0 = (\omega' + j\omega'')\sqrt{\mu\epsilon}$ is complex even for lossless media where ϵ is real. On branch-cut 0

$$\begin{aligned} G_v^{(H, BC_0)}(\rho, \omega) &= -\frac{j}{8\pi\epsilon_0} \int_{k_\rho''=-\infty}^{k_\rho''=\text{Im}(k_0)} j dk_\rho'' \\ &\times \left\{ \left[\frac{k_\rho}{-(k_z)_R} + \frac{k_0^2}{-(k_z)_R k_\rho} \right. \right. \\ &\quad \times \left(\frac{-\mu_1(k_z)_R - \mu_0 k_{1z}}{-\mu_1(k_z)_R + \mu_0 k_{1z}} \right) \\ &\quad \left. - \frac{(k_z)_R}{k_\rho} \left(\frac{-\epsilon_1(k_z)_R - \epsilon_0 k_{1z}}{-\epsilon_1(k_z)_R + \epsilon_0 k_{1z}} \right) \right] \\ &\quad \left. \times H_0^{(2)}(k_\rho \rho) \right\}_{k_\rho = k_0 + jk_\rho''} \\ &+ \frac{j}{8\pi\epsilon_0} \int_{k_\rho''=-\infty}^{k_\rho''=\text{Im}(k)} j dk_\rho'' \\ &\times \left\{ \left[\frac{k_\rho}{(k_z)_R} + \frac{k_0^2}{(k_z)_R k_\rho} \right. \right. \\ &\quad \times \left(\frac{\mu_1(k_z)_R - \mu_0 k_{1z}}{\mu_1(k_z)_R + \mu_0 k_{1z}} \right) \\ &\quad \left. + \frac{(k_z)_R}{k_\rho} \left(\frac{\epsilon_1(k_z)_R - \epsilon_0 k_{1z}}{\epsilon_1(k_z)_R + \epsilon_0 k_{1z}} \right) \right] \\ &\quad \left. \times H_0^{(2)}(k_\rho \rho) \right\}_{k_\rho = k_0 + jk_\rho''}. \end{aligned}$$

Simplifying the R_{01}^{TE} terms

$$\frac{-\mu_1(k_z)_R - \mu_0 k_{1z}}{-\mu_1(k_z)_R + \mu_0 k_{1z}} + \frac{\mu_1(k_z)_R - \mu_0 k_{1z}}{\mu_1(k_z)_R + \mu_0 k_{1z}} = 2 \frac{[\mu_1(k_z)_R]^2 + (\mu_0 k_{1z})^2}{[\mu_1(k_z)_R]^2 - (\mu_0 k_{1z})^2}.$$

Similarly, for the R_{01}^{TM} terms

$$\frac{-\epsilon_1(k_z)_R - \epsilon_0 k_{1z}}{-\epsilon_1(k_z)_R + \epsilon_0 k_{1z}} + \frac{\epsilon_1(k_z)_R - \epsilon_0 k_{1z}}{\epsilon_1(k_z)_R + \epsilon_0 k_{1z}} = 2 \frac{[\epsilon_1(k_z)_R]^2 + (\epsilon_0 k_{1z})^2}{[\epsilon_1(k_z)_R]^2 - (\epsilon_0 k_{1z})^2}$$

where $(k_z)_R$ indicates the value of k_z on the right branch cut.

Thus

$$G_v^{(H,BC_0)}(\rho, \omega) = \frac{j}{4\pi\epsilon_0} \int_{k''_\rho=-\infty}^{k''_\rho=\text{Im}(k_0)} jdk''_\rho \times \left\{ \left[\frac{k_\rho}{(k_z)_R} + \frac{k_0^2}{(k_z)_R k_\rho} \right] \times \left(\frac{[\mu_1(k_z)_R]^2 + (\mu_0 k_{1z})^2}{[\mu_1(k_z)_R]^2 - (\mu_0 k_{1z})^2} \right) + \frac{(k_z)_R}{k_\rho} \left(\frac{[\epsilon_1(k_z)_R]^2 + (\epsilon_0 k_{1z})^2}{[\epsilon_1(k_z)_R]^2 - (\epsilon_0 k_{1z})^2} \right) \right\} \times H_0^{(2)}(k_\rho \rho) \Big|_{k_\rho=k_0+jk''_\rho}.$$

2) *Integration on Branch-Cut 1:*

$$G_v^{(H,BC_1)}(\rho, \omega) = -\frac{j}{8\pi\epsilon_0} \int_{k''_\rho=-\infty}^{k''_\rho=\text{Im}(k_1)} jdk''_\rho \times \left\{ \left[\frac{k_\rho}{k_z} + \frac{k_0^2}{k_z k_\rho} \left(\frac{\mu_1 k_z + \mu_0(k_{1z})_R}{\mu_1 k_z - \mu_0(k_{1z})_R} \right) + \frac{k_z}{k_\rho} \left(\frac{\epsilon_1 k_z + \epsilon_0(k_{1z})_R}{\epsilon_1 k_z - \epsilon_0(k_{1z})_R} \right) \right] \times H_0^{(2)}(k_\rho \rho) \right\} \Big|_{k_\rho=k_1+jk''_\rho} + \frac{j}{8\pi\epsilon_0} \int_{k''_\rho=-\infty}^{k''_\rho=\text{Im}(k_1)} jdk''_\rho \times \left\{ \left[\frac{k_\rho}{k_z} + \frac{k_0^2}{k_z k_\rho} \left(\frac{\mu_1 k_z - \mu_0(k_{1z})_R}{\mu_1 k_z + \mu_0(k_{1z})_R} \right) + \frac{k_z}{k_\rho} \left(\frac{\epsilon_1 k_z - \epsilon_0(k_{1z})_R}{\epsilon_1 k_z + \epsilon_0(k_{1z})_R} \right) \right] \times H_0^{(2)}(k_\rho \rho) \right\} \Big|_{k_\rho=k_1+jk''_\rho} - \frac{\mu_1 k_z - \mu_0(k_{1z})_R}{\mu_1 k_z + \mu_0(k_{1z})_R} + \frac{\mu_1 k_z - \mu_0(k_{1z})_R}{\mu_1 k_z + \mu_0(k_{1z})_R} = -4 \frac{\mu_1 k_z \mu_0(k_{1z})_R}{(\mu_1 k_z)^2 - [\mu_0(k_{1z})_R]^2}.$$

Hence

$$G_v^{(H,BC_1)}(\rho, \omega) = -\frac{j}{2\pi\epsilon_0} \int_{k''_\rho=-\infty}^{k''_\rho=\text{Im}(k_1)} jdk''_\rho \times \left\{ \left[\frac{k_0^2}{k_z k_\rho} \left(\frac{\mu_1 k_z \mu_0(k_{1z})_R}{(\mu_1 k_z)^2 - [\mu_0(k_{1z})_R]^2} \right) + \frac{k_z}{k_\rho} \left(\frac{\epsilon_1 k_z \epsilon_0(k_{1z})_R}{(\epsilon_1 k_z)^2 - [\epsilon_0(k_{1z})_R]^2} \right) \right] \times H_0^{(2)}(k_\rho \rho) \right\} \Big|_{k_\rho=k_1+jk''_\rho}.$$

B. *Branch-Cut Integration for $G_A^{(H)}$*

In a similar manner in which $G_v^{(H)}$ is derived, $G_A^{(H)}$ can be evaluated to yield the following equations:

$$G_A^{(H,BC_0)}(\rho, \omega) = j \frac{\mu_0}{2\pi} \int_{k''_\rho=-\infty}^{k''_\rho=\text{Im}(k_0)} jdk''_\rho \times \left[k_\rho \frac{\mu_1^2(k_z)_R}{[\mu_1(k_z)_R]^2 - (\mu_0 k_{1z})^2} \times H_0^{(2)}(k_\rho \rho) \right]_{k_\rho=k+jk''_\rho} G_A^{(H,BC_1)}(\rho, \omega) = j \frac{\mu_0}{2\pi} \int_{k''_\rho=-\infty}^{k''_\rho=\text{Im}(k_1)} jdk''_\rho \times \left[k_\rho \frac{\mu_0 \mu_1(k_{1z})_R}{[\mu_0(k_{1z})_R]^2 - (\mu_1 k_z)^2} \times H_0^{(2)}(k_\rho \rho) \right]_{k_\rho=k_1+jk''_\rho}.$$

APPENDIX II

DERIVATION FOR RANGE OF s'' TO ENSURE CONVERGENCE OF FOURIER INTEGRALS IN THE FHT

A. *Ensuring Convergence of $\bar{H}_\nu(s)$*

Referring to (8), as $y \rightarrow \infty$, $e^{ay} \rightarrow \infty$

$$H_\nu(y) \rightarrow \frac{e^{ay}}{e^{\frac{ay}{2}}} = e^{\frac{ay}{2}}.$$

The asymptotic expansion for $J_\nu(z)$ for large z is used in the denominator. For the integrand for $\bar{H}_\nu(s)$ to decay to zero as $y \rightarrow \infty$

$$\begin{aligned} \text{Re}\left(\frac{a}{2} - j2\pi s\right) &< 0 \\ \frac{a}{2} + 2\pi s'' &< 0 \\ s'' &< -\frac{a}{4\pi}. \end{aligned}$$

As $y \rightarrow -\infty$, $e^{ay} \rightarrow 0$, $J_\nu(0) = 0$ except if $\nu = 0$ (which is the concern in this paper), in which case $J_0(0) = 1$. Thus, $e^{ay} e^{-j2\pi s}$ needs to decay

$$\begin{aligned} \text{Re}(a - j2\pi s) &> 0 \\ a + 2\pi s'' &> 0 \\ s'' &> -\frac{a}{2\pi}. \end{aligned}$$

Hence, to ensure convergence of $\bar{H}_\nu(s)$

$$-\frac{a}{2\pi} < s'' < -\frac{a}{4\pi}.$$

B. Ensuring Convergence of $\bar{G}(s)$

Referring to (9), as $y \rightarrow \infty$, $F(Ke^{-ay}) \rightarrow F(0)$. $F(0)$ is, in general, a constant or zero, depending on the function F . Hence, it is necessary to ensure that $e^{-ay}e^{-j2\pi ys} \rightarrow 0$ as $y \rightarrow \infty$

$$\begin{aligned}\operatorname{Re}(-a - j2\pi s) &< 0 \\ -a + 2\pi s'' &< 0 \\ s'' &< \frac{a}{2\pi}.\end{aligned}$$

As $y \rightarrow -\infty$, $F(Ke^{-ay}) \rightarrow F(\infty)$. Suppose that $F(\infty)$ is not 0, then it is necessary for $e^{-ay}e^{-j2\pi ys} \rightarrow 0$ as $y \rightarrow -\infty$

$$\begin{aligned}\operatorname{Re}(a + j2\pi s) &< 0 \\ a - 2\pi s'' &< 0 \\ s'' &> \frac{a}{2\pi}.\end{aligned}$$

This result contradicts the previous result. Thus, it is necessary for $F(\infty)$ to be zero. For the problem to be solved in this paper, $F(\infty)$ does tend to zero.

Thus, to ensure convergence of $\bar{G}(s)$

$$s'' < \frac{a}{2\pi}.$$

REFERENCES

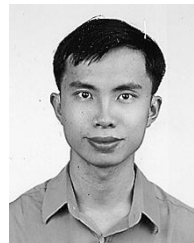
- [1] J. R. Wait, *Geo Electromagnetics*. New York: Academic, 1982.
- [2] D. M. Pozar and D. H. Schaubert, Eds., *Microstrip Antennas: The Analysis and Design of Microstrip Antennas and Arrays*. New York: IEEE Press, 1995.
- [3] J. R. Mosig, "Integral equation techniques," in *Numerical Techniques for Microwave and Millimeter-Wave Passive Structures*, T. Itoh, Ed. New York: Wiley, 1989, ch. 3, pp. 113–213.
- [4] J. A. Fuller and J. R. Wait, "A pulsed dipole in the Earth," in *Transient Electromagnetic Fields*, L. B. Felsen, Ed. New York: Springer-Verlag, 1976, pp. 237–269.
- [5] R. A. Kipp and C. H. Chan, "Complex image method for sources in bounded regions of multi-layer structure," *IEEE Trans. Microwave Theory Tech.*, vol. 42, pp. 860–865, May 1994.
- [6] Y. L. Chow, J. J. Yang, D. G. Fang, and G. E. Howard, "A closed form spatial Green's function for the thick microstrip substrate," *IEEE Trans. Microwave Theory Tech.*, vol. 39, pp. 588–592, Mar. 1991.
- [7] K. A. Michalski and J. R. Mosig, "Multilayered media Green's functions in integral equation formulation," *IEEE Trans. Antennas Propagat.*, vol. 45, pp. 508–519, Mar. 1997.
- [8] S.-Q. Li, Y. Yu, C. H. Chan, K. F. Chan, and L. Tsang, "A sparse-matrix/canonical grid method for analyzing densely packed interconnects," *IEEE Trans. Microwave Theory Tech.*, vol. 49, pp. 1221–1228, July 2001.
- [9] N. B. Christensen, "Optimized fast Hankel transform filters," *Geophys. Prospect.*, vol. 38, pp. 545–568, 1990.
- [10] R.-C. Hsieh and J.-T. Kuo, "Fast full-wave characterization of arbitrary planar microstrip geometries," in *Proc. 1997 Asia-Pacific Microwave Conf*, pp. 685–688.
- [11] —, "Fast full-wave analysis of planar microstrip circuit elements in stratified media," *IEEE Trans. Microwave Theory Tech.*, vol. 46, pp. 1291–1297, Sept. 1998.
- [12] S.-Q. Li, C. H. Chan, L. Tsang, and C.-C. Huang, "Closed-form spatial electric field Green's functions of microstrip structures using the fast Hankel transform and the matrix pencil method," in *Proc Inst. Elect. Eng. . Microwave Antennas and Propagation*, vol. 147, June 2000, pp. 161–166.
- [13] L. Tsang, C.-C. Huang, and C. H. Chan, "Surface electric fields and spatial derivatives of Green's functions of layered media based on half-space extraction," *Microwave Opt. Tech. Lett.*, vol. 24, no. 4, pp. 247–253, Feb. 20, 2000.
- [14] —, "Surface electric fields and impedance matrix elements of stratified media," *IEEE Trans. Antennas Propagat.*, vol. 48, pp. 1533–1543, Oct. 2000.

- [15] R. Achar and M. S. Nakhla, "Simulation of high-speed interconnects," *Proc. IEEE*, vol. 89, no. 5, pp. 693–728, May 2001.
- [16] A. J. Poggio and E. K. Miller, "Integral equation solutions of three dimensional scattering problems," in *Computer Techniques for Electromagnetics*, R. Mittra, Ed. New York: Pergamon, 1973, ch. 4, pp. 159–265.
- [17] B. Shanker, A. A. Ergin, K. Aygün, and E. Michielssen, "Analysis of transient electromagnetic scattering from closed surfaces using a combined field integral equation," *IEEE Trans. Antennas Propagat.*, vol. 48, pp. 1064–1074, July 2000.
- [18] Y. Xu, D. G. Fang, M. Y. Xia, and C. H. Chan, "Speedy computation of the time-domain Green's function for microstrip structures," *Electron. Lett.*, vol. 36, no. 22, pp. 1855–1857, Oct. 2000.
- [19] L. Tsang and D. Rader, "Numerical evaluation of the transient acoustic waveform due to a point source in a fluid-filled borehole," *Geophysics*, vol. 44, no. 10, pp. 1706–1720, Oct. 1979.
- [20] W. C. Chew, *Fields and Waves in Inhomogeneous Media*. New York: IEEE Press, 1995, p. 49, 66, 231.

Leung Tsang (S'73–M'75–SM'85–F'90) was born in Hong Kong. He received the S.B., S.M., and Ph. D. degrees from the Department of Electrical Engineering and Computer Science, Massachusetts Institute of Technology, Cambridge.

He is a Professor of Electrical Engineering at the University of Washington, Seattle, where he has taught since 1983. Since September 2001, he has been on leave from the University of Washington, and is a Professor Chair and Assistant Head of the Department of Electronic Engineering, City University of Hong Kong, Kowloon. He is a coauthor of four books, *Theory of Microwave Remote Sensing* (New York: Wiley-Interscience, 1985), *Scattering of Electromagnetic Waves, Vol. 1: Theory and Applications*, (New York: Wiley Interscience, 2000), *Scattering of Electromagnetic Waves Vol. 2, Numerical Simulations* (New York: Wiley Interscience, 2001), and *Scattering of Electromagnetic Waves Vol. 3, Advanced Topics* (New York: Wiley Interscience, 2001). His current research interests include wave propagation in random media and rough surfaces, remote sensing, high-speed interconnects, computational electromagnetics, wireless communications, and opto-electronics.

Dr. Tsang was the Editor-in-Chief of IEEE TRANSACTIONS ON GEOSCIENCE AND REMOTE SENSING between 1996 and 2001. He was the Technical Program Chairman of the 1994 IEEE Antennas and Propagation International Symposium and the URSI Radio Science Meeting. He was the Technical Program Chairman of the 1995 Progress in Electromagnetics Research Symposium and the General Chairman of the 1998 IEEE International Geoscience and Remote Sensing (GRS) Symposium. He received the IEEE Geoscience and Remote Sensing Society Outstanding Service Award in 2000 and the IEEE Third Millennium Medal in 2000. He is a Fellow of the Optical Society of America and ADCOM member of the IEEE GRS Society.



Chong-Jin Ong (S'01) was born in Singapore. He received the B. Eng. (with first-class honors) and M. Eng. degrees, both in electrical engineering, from the National University of Singapore in 1994 and 1999, respectively. He is currently working toward the Ph.D. degree at the University of Washington, Seattle.

From 1994 to 2001, he was with DSO National Laboratories, Singapore, as an Antenna Engineer. In 2001, he joined the University of Washington, Seattle, as a Research Assistant. His current research

interests include time-domain methods in electromagnetics and signal integrity issues in high-speed interconnects.

Chung-Chi Huang received the B.S. degree in mechanical engineering and the M.S. degree in computer science and engineering from the National Sun Yat-sen University, Kaohsiung, Taiwan, R.O.C., in 1994 and 1996, respectively. He is currently working toward the Ph.D. degree at the University of Washington, Seattle.

His current interests include layered medium Green's function, high-speed interconnects, and computational electromagnetics.

Vikram Jandhyala (S'96–M'98) received the B.Tech. degree in electrical engineering from the Indian Institute of Technology, Delhi, India, in 1993, and the M.S. and Ph.D. degrees in electrical engineering from the University of Illinois, Urbana-Champaign, in 1995 and 1998, respectively.

He is currently an Assistant Professor with the Department of Electrical Engineering, University of Washington, Seattle. From 1998 to 2000, he was a Research and Development Engineer with Ansoft Corporation, Pittsburgh, PA, involved in the acceleration of Ansoft's integral equation solvers. He codeveloped a fast-multipole-based integral equation solver for Ansoft's Spicelink version 4.0, which was released in June 1999. He has published a book chapter and more than 50 journal papers and papers in refereed conference proceedings. His research interests include several aspects of computational and applied electromagnetics, including integral equation techniques, fast computational algorithms, high-speed circuits and devices, signal integrity, rough surface scattering, and radar cross-section computation.

Dr. Jandhyala serves as a Reviewer for several IEEE transactions and conferences. He received an IEEE Microwave Graduate Fellowship in 1997, an Outstanding Graduate Research Award from the University of Illinois in 1998, and a 2001 National Science Foundation CAREER Award. He is a Full Member of the URSI Commission.